Electron-interaction effects on the soft x-ray emission spectra of metals. II. Renormalized theory with application to sodium*†

Shyamalendu M. Bose
Department of Physics and Astronomy, University of Maryland, College Park, Maryland 20742 and Department of Physics, and Atmospheric Science, Drexel University, Philadelphia, Pennsylvania 19104‡

Arnold J. Glick
Department of Physics and Astronomy, University of Maryland, College Park, Maryland 20742
(Received 5 February 1974)

Details of a renormalized theory of the soft x-ray emission spectrum of a light metal are presented. The resulting spectrum shows structure in the plasmon satellite band and the parent band which did not appear in the first-order theory. The structure in the plasmon satellite band arises from the excitation of the plasmaron mode as suggested by Hedin. In addition there is a peak of intensity near the high-energy edge of the parent band, which is related to the threshold effect discussed by Nozières and others. The calculated spectrum differs considerably from what would be expected for noninteracting electrons. It also departs considerably from what could be considered a generalized density of states of the interacting conduction electrons. The transient effect of the disappearance of the core hole makes it impossible to relate the spectrum to the density of states in any simple way. Careful study of the experimental spectra of light metals could serve as a check of the approximations made here, and provide important information about electron correlations in metals.

I. INTRODUCTION

In a previous article[1] we employed many-body perturbation theory to study the effects of electron interactions on the soft x-ray emission spectrum of metals. The emission process is associated with the decay of an electron from a state in the conduction band into a previously created hole in a state of lower energy which is localized around one of the ionic cores. Applying the theory to the $L_{2,3}$ emission of sodium and going to first order in the effective interaction between particles, the spectrum was found to have a low-energy tail and a plasmon satellite band. In agreement with the experimental results of Rooke,[2] the maximum intensity of the satellite band was found to reach 2% of that of the parent band. The intensity of the low-energy tail also was found to be of this magnitude in the region of the satellite band. However, the comparison of intensities had to be made with the parent band calculated from the one-electron model without interactions. The first-order theory could not be used for the parent band because of the appearance of divergent terms. Here we present the results obtained using a renormalized theory which is free of this difficulty.

It is found that the plasmon satellite band and the parent band have structures which did not appear in first order. Hedin[3] suggested that there should be a peak in the emission spectrum due to a collective mode called the plasmaron.[4] The structure we find in the plasmon satellite band appears to be associated with this effect though the presence of the hole in the core state makes it weaker than originally predicted. In addition, there is a peak of intensity near the high-energy edge of the spectrum. Such a peak has already been observed in the spectrum of sodium and perhaps other metals.[5] Here we trace its origin to an instability of the electron gas around the transient hole in the localized core state. This peak is related to the one recently discussed by Nozières and others[6-9] using a simplified model of the radiation process.

In Sec. II we study the nature and origin of the divergences of the first-order theory and consider the modifications of the theory required to account for the strong interactions of the particles or holes with the charge clouds which surround them. We shall see that the calculation can still be represented by Feynman-type diagrams analogous to those shown in Fig. 1, but now the conduction and core particle lines must be renormalized to include the cloud effects. We sketch the calculation in Sec. III and in Sec. IV we summarize our results and compare the theory with several other treatments of the x-ray emission spectra which have recently appeared.

II. DIVERGENCES AND RENORMALIZATIONS

In I the x-ray emission intensity was found from the transition rate for the interacting many-electron system to undergo radiative decay from its initial state with a deep-lying hole localized about one ionic core. The transition rate was then re-

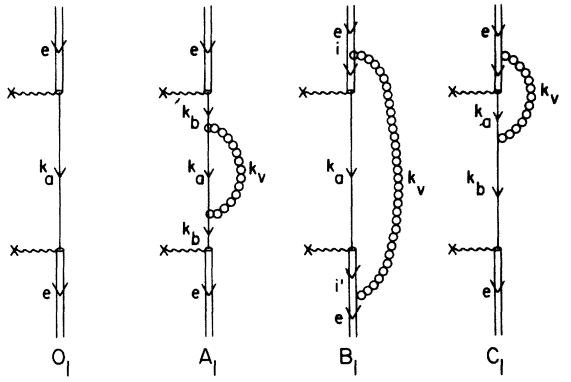

FIG. 1. Zero-order and first-order diagrams contributing to x-ray emission.

lated to a series of Feynman-type diagrams. To first order in the effective interaction between particles the important diagrams which contributed are those reproduced in Fig. 1. Diagram 0_1 is the zero-order contribution which is equivalent to the one-electron model. All three first-order graphs, A_1, B_1, and C_1, present difficulties when one extends the calculation to frequencies for which 0_1 does not vanish, namely, the region

$$|E_B| \leq \hbar\omega \leq |E_B| + E_F , \tag{1}$$

where E_B is the energy of the initial hole below the bottom of the conduction band, and E_F is the Fermi energy. The contribution of graph A_1 will be seen to be meaningless in this region, B_1 diverges logarithmically everywhere within this frequency range, and C_1 diverges at the high-energy edge of the emission spectrum.

The contribution from A_1 contains an integral whose integrand is of the form [see Eq. (24a) of I]

$$\Delta \frac{\partial}{\partial E_b}\left(\frac{1}{\omega + E_B - E_b - i\lambda}\right) , \tag{2}$$

where Δ is a factor which depends on the electron-electron interaction, E_b is a conduction-electron energy, and $\lambda \to 0$. Note that A_1 differs from 0_1 only by an interaction "self-energy" part inserted into the conduction-electron line. Higher-order graphs in which there are more self-energy parts inserted into this conduction-electron line are even more singular at this point. The origin of the difficulty can be understood by noting that the interparticle interaction introduces shifts in the energy of the single-particle states, and A_1 can be identified as the first-order term in a Taylor-series expansion of a denominator assuming that the shifts are small. However, the expansion is meaningless near poles of the denominator. Since the poles occur within the region of integration whenever ω satisfies Eq. (1), we see that A_1 cannot give an adequate representation of the self-energy processes once we leave the tailing region of the spectrum and enter the main band. The energy shifts can, however, be introduced consistently into the theory by replacing in 0_1 the bare conduction electron by a dressed particle in the familiar way. Then the propagator $S_F(\vec{k}_a, \omega)$ defined in Eq. (B2) of I is replaced by a renormalized form, $\mathcal{S}_F(\vec{k}_a, \omega)$, as indicated in Fig. 2. Explicitly one has

$$\mathcal{S}_F(\vec{k}_a, \omega) = \frac{i}{\omega - E_a - \Sigma(\vec{k}_a, \omega)} , \tag{3}$$

where $\Sigma(\vec{k}_a, \omega)$ is the complex frequency and wave-number-dependent self-energy, which here is taken in the random-phase approximation (RPA).

The contribution B_1 was studied in I and shown to diverge logarithmically throughout the main-band region. The physical origin of this divergence is quite interesting. The hole in the core state which is formed prior to the x-ray emission, acts as a localized impurity to the conduction electrons of the metal and thus destroys the translational symmetry of the problem. The impurity potential can then scatter electrons unrestricted by momentum conservation. Among these scatterings are those in which electrons from occupied states very close to the Fermi surface are transferred to unoccupied states which are also very close to the Fermi surface. The energy of such excitations is arbitrarily small though the momentum change of electrons can be as large as $2k_F$. Thus it appears that a large number of very low-energy electron-hole pairs can be created without much loss of energy. This effect gives rise to an infrared type of divergence in the x-ray emission process. Of course, it is different from an ordinary infrared divergence in that the low-energy particles are not photons, but rather fermion particle-

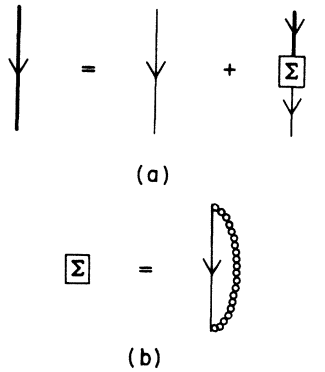

FIG. 2. Diagrammatic representation of the integral equation satisfied by the interacting conduction-electron propagator. Self-energy calculated in the RPA with an electron or hole in the intermediate state.

hole pairs. Actually, this process of pair formation should be self-limiting. As the pairs are formed, they should form a screening cloud which would inhibit further pair excitation. This means that the noninteracting propagator for the core-hole state which has been used in I is not the proper one to use. The state must always be considered together with its interaction self-energy. We incorporate the effect of the presence of the screening cloud into the theory by introducing a renormalized core-state propagator. The renormalization procedure is shown diagrammatically in Fig. 3. Figure 3(a) is the graphical representation of the Dyson's equation satisfied by the renormalized bound-state propagator. Then the propagator of Eq. (B3) in I is replaced by

$$g_B(\omega)=\frac{i}{\omega-E_B-\Sigma_B(\omega)}\,. \tag{4}$$

The self-energy $\Sigma_B(\omega)$ is calculated to first order in the effective electron-electron interaction as indicated in the first two graphs on the right-hand side of Fig. 3(b). The effective interaction accounts for conduction-electron-hole excitations as described in I. The self-energy thus contains the effect of Auger excitation as well as virtual scattering off the localized hole. The third contribution in Fig. 3(b) is a radiative correction to the self-energy, but it will be shown in the Appendix to be much weaker than the electron-electron contribution. For consistency, the initial-hole state is also considered along with its cloud of particle-hole pairs. The observed energy E_B' of this state then includes the real part of the self-energy evaluated on the energy shell

$$E_B'=E_B+\mathrm{Re}\Sigma_B(E_B)\,, \tag{5}$$

and a width $\Gamma_B=\mathrm{Im}\Sigma_B$. Since, as we will see below, Γ_B is quite small, we will be able to neglect its effect on the initial state,[10] while the energy shift $\mathrm{Re}\Sigma_B(E_B)$ will play an important role in partially cancelling the off-energy shell shift coming from $\Sigma_B(\omega)$.

In a recent study of the x-ray emission and absorption problems with a two-Hamiltonian model[6-8] Bergersen *et al.*[11] claim that the B_1 term is not divergent in their modified first-order theory. They find an extra term arising from the mixed normalization of the many-body states with two Hamiltonians, and this term cancels the divergence. In our approach, we use a single, though more complicated, Hamiltonian in which case the formalism automatically accounts for normalization. However, a term of the type found in Ref. 11 could be inferred[12,13] as coming from other highly divergent graphs, those with initial- or final-state self-energies [Figs. 4(D) and 7(D) of I]. These graphs were perhaps erroneously argued away in I. The exact form of this additional term, however, is ambiguous and depends on the limiting procedure used to obtain it. In the "first-order" renormalized theory used here, there remain some ambiguities on this point as will be discussed elsewhere.[13] However, it appears that the renormalized correction terms are small and, whichever form is used or even if these terms are neglected, there will be little change in the final spectrum.

Finally we must consider the "interference graphs" C_1. These terms are also affected by the infrared process, though in a different way. The singular terms are associated with the particular time ordering shown in Fig. 4. When the difference in energy between the conduction hole and the conduction electron becomes vanishingly small the x-ray intensity diverges logarithmically. Since this can only happen for electrons and holes at the Fermi surface, the divergence occurs at the high-energy threshold of the spectrum

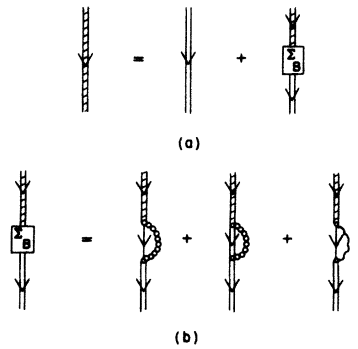

FIG. 3. (a) Integral equation for the interacting bound-state propagator. (b) The self-energy has a radiative part and an electron interaction part with the intermediate hole in either the core or the conduction band.

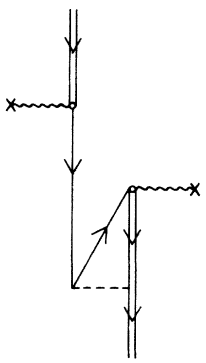

FIG. 4. Particular time ordering of the interference graph causing logarithmic divergence of the x-ray intensity.

$\omega = |E_B'| + E_F$. However, if the bound state is shielded by a cloud of particle-hole pairs the divergence is eliminated (though we will see that it leaves a residual observable effect).

In I we say that in the tailing and plasmon satellite regions C_1 tends to cancel the contributions A_1 and B_1. When these terms are renormalized, care must be taken to include a consistent set of processes, otherwise these delicate cancellations can be lost. Figure 5 shows the renormalized graphs which we consider in this paper, and which will preserve this cancellation. It will be noticed that some unrenormalized electron lines still appear in contributions B, C_1, and C_2. While it would, in principle, be desirable to correct these lines also, the calculations would become much more difficult. The omitted corrections would be needed to describe the double-plasmon satellite band. However, this band is expected to be very weak and its detection would be difficult. Also it occurs at low energies—down from the main band by at least twice the plasmon energy. In the region of present interest the omitted terms are not expected to have significant quantitative or qualitative effect.

While the graphs of Fig. 5 preserve the cancellation between terms found in the first-order theory, there may be other contributions which are needed to preserve other consistency requirements. The importance of choosing consistent sets of graphs has been pointed out by Baym and Kadanoff[14] and others. For the x-ray emission problem Rystephanick and Carbotte[15] and Nozières *et al.*[7,16] have stressed the importance of some additional terms which we do not include in the present calculation. These enter in the form of higher-order vertex corrections to Fig. 5, C_1 and C_2. These additional corrections play an important role in determining the analytic structure of the emission intensity near the high-energy threshold of the spectrum. At lower energies their main effect is as an over-all multiplicative

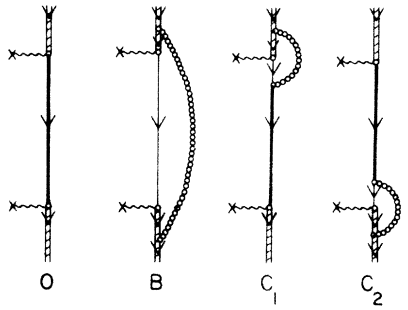

FIG. 5. Renormalized diagrams contributing to the x-ray emission intensity.

factor which sets the absolute value of the intensity. Since the experiments measure only relative intensities, these terms will have little practical effect except near the threshold. We will return to this point in Sec. IV.

III. CALCULATION

We saw in I that the x-ray emission intensity can be obtained from [Eq. (I3)]

$$I(\omega) = \frac{\omega}{\pi l} \operatorname{Re} F(\omega) , \tag{6}$$

where [Eq. (I5)]

$$F(\omega) = \sum_i \int_0^\infty dt\, e^{-i\omega t} \langle \Psi_i | \theta^\dagger(t)\theta(0) | \Psi_i \rangle , \tag{7}$$

with

$$\theta(t) = e^{iHt} \sum_{k=1}^{N} \vec{n}\cdot\vec{p}_k e^{-iHt} .$$

We can now proceed to the calculation of the correlation function $F(\omega)$ from the diagrams of Fig. 5 obtained by using the renormalized theory of Sec. II. The rules for writing down the contributions of these diagrams have been discussed in Appendix A of I. Following these rules, we obtain the following contributions to $F(\omega)$ from the graphs A, B, C_1, and C_2 of Fig. 5,

$$F_A(\omega) = -\frac{i}{2\pi} \int \frac{d\omega'}{\omega' - \omega + i\lambda} \sum_{k_a} \mathcal{S}_F(\vec{k}_a, E_B' + \omega') \sum_{e=1}^{3} |h_{\vec{n},e}(\vec{k}_a)|^2 , \tag{8}$$

$$F_B(\omega) = \frac{1}{(2\pi)^2\Omega} \int \frac{d\omega'}{\omega' - \omega + i\lambda} \int d\omega_v \sum_{\vec{k}_v} \sum_{\vec{k}_a} V(\vec{k}_v, \omega_v)[\mathcal{S}_B(E_B' + \omega_v)]^2$$
$$\times S_F(\vec{k}_a, E_B' + \omega' + \omega_v) \sum_e \left| \sum_i g_{ie}(\vec{k}_v) h_{\vec{n},e}(\vec{k}_a) \right|^2 , \tag{9}$$

$$F_C(\omega) = -\frac{2}{(2\pi)^2\Omega} \int \frac{d\omega'}{\omega' - \omega + i\lambda} \int d\omega_v \sum_{\vec{k}_v} \sum_{\vec{k}_a} \sum_{\vec{k}_b} V(\vec{k}_v, \omega_v)\mathcal{S}_B(E_B' - \omega_v)$$
$$\times S_F(\vec{k}_a, E_B' + \omega' + \omega_v)\mathcal{S}_F(\vec{k}_v, E_B' + \omega')\delta_{\vec{k}_a, \vec{k}_b + \vec{k}_v} \sum_{i,e} g_{ie}(\vec{k}_v) h_{\vec{n},i}(\vec{k}_a) h_{\vec{n},e}(\vec{k}_b) . \tag{10}$$

Term $F_C(\omega)$ contains an extra factor of 2 to account for the presence of both C_1 and C_2. The dynamic Coulomb interaction between electrons (the line of bubbles) is represented by $V(\vec{k}_v, \omega_v)$; the matrix element for interaction with the radiation field (the wavy line) is $h_{\vec{n},i}(\vec{k}_a)$ where $\vec{k}_a$ is the wave number of the incoming or outgoing conduction electron; $g_{ie}(\vec{k}_v)$ with momentum $\vec{k}_v$ occurs for the vertex in which a line of electron interaction joins an incoming and an outgoing bound-state hole. $S_F(\vec{k}, \omega)$ is the noninteracting conduction-electron-hole propagator. All of these quantities have been explicitly defined in I. In addition $\mathcal{S}_F(\vec{k}, \omega)$ and $\mathcal{S}_B(\omega)$ are the renormalized conduction-electron and core-state propagators, respectively, and they can be conveniently expressed in terms of spectral functions:

$$\mathcal{S}_F(\vec{k}, \omega) = \int_{-\infty}^{\infty} \frac{d\omega'}{\pi} \left(\frac{i\theta(\omega' - E_F)}{\omega - \omega' + i\lambda} + \frac{i\theta(E_F - \omega')}{\omega - \omega' - i\lambda} \right) \times \frac{\Sigma_2(\vec{k}, \omega')}{[\omega' - E_k - \Sigma_1(\vec{k}, \omega')]^2 + \Sigma_2(\vec{k}, \omega')^2} , \tag{11}$$

where $\Sigma_1(\vec{k}, \omega)$ and $\Sigma_2(\vec{k}, \omega)$ are the real and imaginary parts of the conduction-electron self-energy as defined in Fig. 2 and they satisfy the following dispersion relation:

$$\Sigma_1(\vec{k}, \omega) = \Sigma_{ex}(\vec{k}) + P \int_{-\infty}^{\infty} \frac{d\omega'}{2\pi} \frac{\Sigma_2(\vec{k}, \omega)}{\omega - \omega'} , \tag{12}$$

where $\Sigma_{ex}(\vec{k})$ is pure real and frequency independent,

$$\Sigma_{ex}(\vec{k}) = -\frac{h^2 k_F}{\pi m a_0} \left(1 + \frac{k_F^2 - k^2}{2kk_F} \ln \left| \frac{k + k_F}{k - k_F} \right| \right) . \tag{13}$$

Similarly

$$\mathcal{S}_B(\omega) = \int_{-\infty}^{\infty} \frac{d\omega'}{\pi} \frac{i}{\omega - \omega' - i\lambda} \times \frac{\Gamma_B(\omega')}{[\omega' - E_B - \Sigma_B(\omega')]^2 + \Gamma_B^2(\omega')} , \tag{14}$$

where $\Sigma_B(\omega)$ is the real part and $\Gamma_B(\omega)$ is the imaginary part of the bound-state self-energy. Now using these definitions we can carry out the integrations over ω' and ω_v. After integrating and substituting into Eq. (6) we obtain for the intensity of emission:

$$I_A(\omega) = \frac{\omega}{3\pi} \sum_{\vec{k}_a} \theta(E_F - \omega - E_B') \operatorname{Im} \left(\frac{\mathcal{S}_F(\vec{k}_a, \omega + E_B')}{i} \right) \sum_{e=1}^{3} |h_{\vec{n},e}(\vec{k}_a)|^2 , \tag{15a}$$

$$I_B(\omega) = -\frac{\omega}{3\pi\Omega} \sum_{\vec{k}_v} \sum_{\vec{k}_a} \eta_{\vec{k}_a <} \left[\operatorname{Im} V_-(\vec{k}_v, \omega + E_B' - E_a) [\operatorname{Re} \mathcal{S}_B(E_a - \omega)/i]^2 - \frac{2P}{\pi} \int_{-\infty}^{\infty} \frac{d\omega'}{E_a - \omega - \omega'} \operatorname{Im} V_-(\vec{k}_v, E_B' - \omega') \times \operatorname{Re} \left(\frac{\mathcal{S}_B(\omega')}{i} \right) \operatorname{Im} [\mathcal{S}_B(\omega')/i] \right] \sum_{i=1}^{3} \left| \sum_{e=1}^{3} g_{ie}(\vec{k}_v) h_{\vec{n},e}(\vec{k}_a) \right|^2 , \tag{15b}$$

$$I_C(\omega) = \frac{\omega}{3\pi\Omega} \sum_{\vec{k}_v} \sum_{\vec{k}_a} \sum_{\vec{k}_b} \left[\eta_{\vec{k}_a <} \operatorname{Im} V_-(\vec{k}_v, \omega + E_B' - E_a) \operatorname{Re} \left(\frac{\mathcal{S}_F(\vec{k}_a, \omega + E_B')}{i} \right) \times \operatorname{Re} \left(\frac{\mathcal{S}_B(E_b - \omega)}{i} \right) - \operatorname{Re} \left(\frac{\mathcal{S}_B(E_b - \omega)}{i} \right) \operatorname{Im} \left(\frac{\mathcal{S}_F(\vec{k}_a, \omega + E_B')}{i} \right) \theta(E_F - \omega - E_B') \times [\operatorname{Re} V_-(\vec{k}_v, 0) + \eta_{\vec{k}_b >} \operatorname{Re} V_+(\vec{k}_v, \omega + E_B' - E_b) - \eta_{\vec{k}_b <} \operatorname{Re} V_-(\vec{k}_v, \omega + E_B' - E_b)] \right] \times \delta_{\vec{k}_a, \vec{k}_v + \vec{k}_b} \sum_{i=1}^{3} \sum_{e=1}^{3} g_{ie}(\vec{k}_v) h_{\vec{n},i}(\vec{k}_a) h_{\vec{n},e}(\vec{k}_b) , \tag{15c}$$

where

$$\operatorname{Im} \left(\frac{\mathcal{S}_F(\vec{k}_a, \omega + E_B')}{i} \right) = \frac{\Sigma_2(\vec{k}_a, \omega + E_B')}{[\omega + E_B' - E_a - \Sigma_1(\vec{k}_a, \omega + E_B')]^2 + \Sigma_2(\vec{k}_a, \omega + E_B')^2} ,$$

$$\operatorname{Re} \left(\frac{\mathcal{S}_B(\omega)}{i} \right) = \frac{\omega - E_B - \Sigma_B(\omega)}{[\omega - E_B - \Sigma_B(\omega)]^2 + \Gamma_B(\omega)^2} ,$$

$$\operatorname{Im} [\mathcal{S}_B(\omega)/i] = \frac{\Gamma_B(\omega)}{[\omega - E_B - \Sigma_B(\omega)]^2 + \Gamma_B(\omega)^2} .$$

Equation (15a) replaces Eqs. (I23) and (I24a) of I, and Eqs. (15b) and (15c) replace Eqs. (I24b) and (I24c), respectively. The second term of Eq. (15b) does not contribute significantly to the emission process compared to the first term and hence can be neglected. Its smallness is a consequence of the fact that $\Gamma_B(\omega')/4E_F \sim 10^{-4}$, as demonstrated in Appendix A. Hence the second term, which contains a factor of Γ_B in the numerator, is expected to be negligible unless the denominator vanishes. Indeed, Eq. (15b) includes the process shown in Fig. 1 B_1 which led to the troublesome infrared divergence in the energy band $|E'_B| < \hbar\omega < |E'_B| + E_F$, i.e., in the region of the parent band. However, after renormalization (i.e., the inclusion of an infinite set of higher-order terms) Eq. (15b) no longer is divergent. The quasiparticle core state has a finite lifetime so that even when $\omega + E'_B = E_a$, the denominator does not become zero because the real part $\Sigma_B(E_a - \omega)$ does not go to zero at the same frequency as does $\Gamma_B(E_a - \omega)$. Hence, renormalization of the bound-state propagator eliminates the troublesome infrared divergence from our problem. Note that even at the high-energy threshold, the spectrum will not be singular since, although $\Gamma_B = 0$ at E_F (see Table III), for computing the behavior at the threshold we only need Γ_B at E'_B where it is not zero.

$I_A(\omega)$ passes smoothly through $\hbar\omega = |E'_B|$, the zero-order emission edge. Thus by including a renormalized conduction-electron propagator we have been able to remove the unphysical discontinuity in slope at the threshold of the so-called parent emission band. Also we note that introduction of renormalization in our problem has removed all the δ-function restrictions in energy that were present in Eq. (I24) and in this case all the terms in Eqs. (15a)–(15c) will contribute everywhere in the spectrum, i.e., in the parent band, tailing region, and the plasmon satellite band.

We have carried out the integrations over the angles of the momenta in Eqs. (15a)–(15c) analytically. In order to proceed further one needs the real and imaginary parts of conduction-electron self-energies and also the bound-state self-energies.

The numerical calculation of the imaginary part of the conduction-electron self-energy has already been carried out.[17] We have neglected $\Sigma_1(\vec{k}, \omega)$ for the calculation of the spectrum in the main-band region, since Σ_1 does not have any important structure in this frequency region and is not expected to change the shape of the spectrum by any appreciable amount. For the calculation of the plasmon satellite band and the tailing, however, the real part of the self-energy must be retained. Hedin, Lundqvist, and Lundqvist[3,4,18] were the first to point out the important role of this term in modifying the low-energy portion of the spectrum. As a consequence of Eq. (12) the rapid variation in $\Sigma_2(\vec{k}, \omega)$ is associated with corresponding variation in $\Sigma_1(\vec{k}, \omega)$. This behavior is indicated in Fig. 1 of Ref. 18 for a particular value of momentum $\vec{k}$. Note that there are denominators in Eqs. (15a) and (15c) which tend to be small and would vanish at certain points if not for $\Sigma_2(\vec{k}_a, \omega + E'_B)$. These points correspond to those marked on Fig. 1 of Ref. 18 as the intersections of the straight line $\omega - E^*_k$ with $\Sigma_1(\vec{k}, \omega)$. The high-frequency intersection is only weakly shifted from the free-particle pole at $\omega = E_k$. The central intersection is not too important because it occurs where $\Sigma_2(\vec{k}, \omega)$ is large. The low-frequency crossing leads to an additional peak in the spectral function of the renormalized single-particle Green's function. This peak is the "plasmaron" of Hedin, Lundqvist, and Lundqvist,[4] which they interpret as a coupled plasmon-hole mode. For the x-ray emission spectrum one must integrate over different values of the momentum $\vec{k}_a$, and the effect of this peak is partially smeared out. However, a residual peak does persist in the spectrum and we will see that it occurs near the low-energy side of the plasmon satellite band.

The real and imaginary parts of the core-state self-energy are obtained from Eqs. (A1), (A2), and (A3) of the Appendix. However, we note that $\Gamma_{B2}(E_a - \omega)$ will not contribute to $I_B(\omega)$. From Eq. (A2) it is clear that $\Gamma_{B2}(E_a - \omega)$ will be zero unless $E_a < \omega + E'_B$. But the factor $\mathrm{Im}V_-(\vec{k}_v, \omega + E'_B - E_a)$ in Eq. (15b) requires $\omega + E'_B < E_a$. The radiation contribution $\Gamma_{B3}(E_a - \omega)$ is not zero, but, as shown in the Appendix, it is weaker by a factor 10^3 than the main Auger term $\Gamma_{B1}(E_a - \omega)$, and can be neglected. Again we shall be interested in frequencies less than the Fermi energy, hence the term containing $\mathrm{Im}V_+(\vec{k}_v, \omega - E_a)$ in $\Gamma_{B1}(E_a - \omega)$ will not contribute.

Using the numerical values of real and imaginary parts of the self-energy of the conduction electron and core-state propagators, we have carried out the final single integral of $I_A(\omega)$, double integral of $I_B(\omega)$, and the three and four-dimensional integrals of $I_C(\omega)$ numerically with the aid of an IBM 7094 computer. Contributions to the emission intensity by $I_A(\omega)$, $I_B(\omega)$, and $I_C(\omega)$ in the main-band region are shown in Table I, and the total contribution for the plasmon satellite region in Table II. The total contributions for the main band and satellite band are then plotted in Fig. 6. The dashed line in this figure is the experimental result of Skinner[19] and the solid lines represent the results of our calculations both in the main-band and the satellite-band regions.

TABLE I. Contributions to the main emission band and tail from the graphs of the renormalized theory.

$\frac{\omega+E_B}{4E_F}$	I_A	I_B	I_C	I_{Tot}
−0.10	0.0115	0.0102	0.0068	0.0285
−0.05	0.0166	0.0126	0.0129	0.0421
0.	0.0359	0.0208	0.0440	0.1007
0.025	0.0530	0.0284	0.0772	0.1586
0.05	0.0757	0.0325	0.1304	0.2386
0.075	0.0955	0.0353	0.1854	0.3162
0.10	0.1131	0.0375	0.2185	0.3691
0.125	0.1248	0.0390	0.2524	0.4162
0.15	0.1358	0.0401	0.2784	0.4543
0.175	0.1448	0.0408	0.3049	0.4905
0.20	0.1524	0.0405	0.3501	0.5430
0.225	0.1583	0.0369	0.3949	0.5901
0.24	0.1618	0.0268	0.4411	0.6297
0.245	0.1627	0.0230	0.4608	0.6465

IV. SUMMARY AND CONCLUSIONS

The renormalization of the particle and hole propagators, as carried out in the previous sections, removes fundamental shortcomings of the first-order theory and introduces interesting new structures into the emission spectrum. Replacement of the basic electron and the core-hole states by quasiparticles considered along with their clouds of interacting particles removes the logarithmic divergences in the main-band region. However, a residual effect seems to persist, giving structure to the high-energy threshold. We observe from Fig. 6 that our results agree quite well with the experimental observation of Skinner.[19] The calculated curve follows the experimental curve very closely over most of the tailing and the parabolic region of the main emission band, though our calculation indicates a stronger peak near the high-energy edge. This peak occurs due to the infrared effect which has been discussed in Sec. II. In fact, if we did not include the lifetime of the core-hole state we would obtain a singularity at this edge of the spectrum, not unlike that in the Kondo effect.[20] Our calculation of this effect is limited in that other higher-order graphs can be important in this region. However the present calculation includes the finite lifetime of the core hole which other calculations neglected. To obtain the correct analytic structure at the edge, both factors, i.e., the higher-order graphs and the lifetime effects must be accounted for. Without lifetime, the theory would imply a singular behavior $(E-E_F)^{-\alpha}$ near the threshold. An unrenormalized theory would give $\alpha \ln (E-E_F)$ as a first-order approximation to this term. However, in the renormalized theory where the lifetime of the core propagators are included, the threshold behavior should be something like $\frac{1}{2}\alpha \ln[(E-E_F)^2 + \Gamma_B(E_B')^2]^{1/2}$. Thus at the threshold although our spectrum shows a sharp peak, it is not strictly singular because of finite lifetime of the core propagator. The spectrum obtained by Cady and Tomboulian[21] has no rise at this energy, though there is some evidence of a peak in both Skinner's[19] and Crisp and William's[5] result. Recent calculations by Nozières *et al.*,[7,8] Mahan,[6] and others with a model Hamiltonian which only includes the scattering of conduction electron by the transient core potential (neglecting conduction-electron–conduction-electron interactions) have suggested that there should indeed be a Kondo-like singularity at these energies for the $L_{2,3}$ emission spectrum, and the divergence remains as long as the Fermi surface is sharp. For temperatures above absolute zero the divergence is removed,[22] with kT playing a role similar to that of Γ_B in the present theory. Since the emis-

TABLE II. Plasmon satellite band obtained from the renormalized theory.

$\frac{\omega+E_B}{4E_F}$	I_{Tot}^{P1}
−0.215	0
−0.225	0.0133
−0.25	0.0230
−0.30	0.0322
−0.35	0.0342
−0.40	0.0303
−0.45	0.0254
−0.50	0.0132
−0.52	0.0120
−0.55	0.0094
−0.60	0.0102
−0.625	0.0009
−0.65	0.0001
−0.70	0.

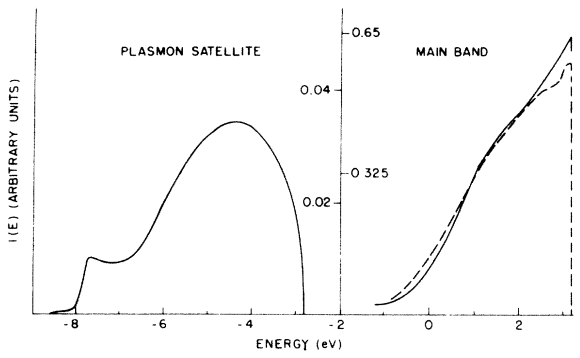

FIG. 6. Main emission band and plasmon satellite band from the renormalized theory. The dashed curve represents Skinner's experimental result. The plasmon satellite shows some residual plasmaron structure.

sion intensity near the high-energy edge would be strongly affected by self-absorption and the resolving power of the detector, a peak should become more apparent in more careful experiments eliminating these effects. The width of this high-energy peak can give a measure of the internal Auger broadening, and the effective temperature in the neighborhood of the localized core state.

We observe that the calculated spectrum differs considerably from what would be expected from the Sommerfeld theory of noninteracting electrons. The $E^{1/2}$ behavior coming from the density of states of noninteracting electrons seems to persist only in a small region at the middle of the emission band. It has been proposed that the spectrum gives a direct reflection of a generalized interaction density of states of the electrons.[3] However, such an interpretation is subject to question and must be used with care. The density of states of the conduction electrons is different in the initial and final states due to the disappearance of the bound-state hole. It is not obvious which generalized density of states is the one to be introduced into the soft x-ray spectrum. In fact, the spectrum includes features related to the time evolution of the density of states from its initial to its final form. The peak at the high-energy threshold can be interpreted as being one such effect. It enters the present calculations via the dynamic scattering of conduction electrons by the bound-hole potential [such as in Fig. 5(c)]. Terms of this type are not adequately treated in Ref. 3. Indeed, they neglect all dynamical correlations between the hole and the conduction electrons. It may not be a simple matter to separate these "anomalous" effects in the observed spectra from those of the generalized density of states.

These terms also have a strong effect on the absolute magnitude of the emission intensity. The contribution of the various interaction diagrams is larger than the zero-order result of the Sommerfeld model. There is a considerable readjustment of electron density in the vicinity of the positively charged core hole, the density becoming larger than the average electron density in other parts of the metal. Thus, it is not surprising that these terms will give rise to an emission intensity which exceeds the Sommerfeld or the zero-order result. The same effect has been observed in the calculation of the positron annihilation in metals. The problem of positron annihilation has many features in common with the soft x-ray emission process. The positron in an electron gas plays essentially the same role as the initial hole in the core state and the total positron annihilation rate is found to be greatly enhanced over the Sommerfeld values due to a distortion of the conduction-electron configurations by the positron.[23]

As in the first-order theory the plasmon satellite band has its high-energy edge shifted by an energy $\hbar\omega_p$ below the high-energy edge of the parent band. Because of the presence of dispersion in the plasmon frequency and the cancellation between different terms, the main peak in the plasmon band becomes broad and gets shifted to lower energies. Very close to the high-energy threshold of the plasmon band the intensity should behave as $(E_0 - E)^{3/2}$ as pointed out by Ferrell,[24] where $E_0 = |E_B^l| + E_F - \hbar\omega_p$ is the threshold energy. This behavior is not obvious in Fig. 6, but should be apparent when the numerical calculations are carried out on a finer mesh and plotted using an expanded scale.[25] Apart from this broad peak the renormalized theory introduces an additional structure to the satellite band. A secondary peak of lower intensity is found to occur towards the lower-energy edge of the satellite band, which was definitely not present in the first-order theory. The existence of such a structure in the satellite band has been predicted by Hedin *et al.*,[3,4] and is due to structure in the real part of the electron self-energy as discussed in Sec. III.[26] Hedin suggests that such a secondary peak is obtained because of the existence of a new elementary excitation in an electron gas, occurring due to the resonant interaction of a plasmon-type oscillation with a hole in the conduction band. This new excitation is called a plasmaron and has a larger energy than a free plasmon. Attempts by Cuthill *et al.*[27] to observe this structure experimentally in aluminum have not yet been able to definitely resolve it from background noise.

Since the experiments only provide relative intensities it is interesting to compare the magnitude of the intensity of the main band and of the plasmon satellite band. As mentioned before, one of the important effects of the presence of a hole in the core state is to increase the magnitude of the intensity over the Sommerfeld value in the main-band region. Our numerical results show that the total intensity is enhanced by about a factor of 4. However, as observed in I, the hole in the core state introduces very strong cancellation among contributions for the satellite band and reduces the maximum intensity by a factor of about 20. This cancellation is somewhat lost in the renormalized theory. The intensity of the satellite band is found to increase by a factor of about 6. The peak of the plasmon satellite band thus becomes roughly 5% of the maximum intensity of the main emission band. Hedin[3] has pointed out that when Rooke's raw experimental data are expressed

in our units it gives the ratio as 4%. So the result of the renormalized theory seems to be in better agreement with experiment than the first-order theory as to this feature of the spectrum.

After this work was initially reported,[28] some related work was published by Morita and Watabe.[29] They also use a Green's function method to study the x-ray emission spectra of light metals, and in principle, they discuss the same processes considered here. However, their actual numerical calculations appear to be more limited. Devoting their primary attention to the main band they carried out detailed calculations only for the term in Fig. 5(a). This calculation thus corresponds to the generalization of Landsberg's calculation.[30] They use extrapolation formulas for the real and imaginary parts of the self-energy of the conduction electrons and obtain results which are also qualitatively very similar to Landsberg's. While leaving out the equally large numerical contributions of Figs. 5(b) and 5(c) they appear to go beyond the present calculation in their consideration of the hump near the high-energy threshold. Using a statically screened Coulomb interaction they have considered a whole set of vertex corrections in addition to Fig. 5(c). These enter as a set of diagrams containing ladder interactions and crossed ladders. Following Mahan[6] they find that near the high-energy edge the spectrum should indeed rise. However, no actual numerical results are performed with this model. Also, Nozières and co-workers[7,8,16] have now shown that a whole class of additional terms must be included [analogous to, and beyond Fig. 5(b)] in order to give an adequate treatment to this feature of the spectrum.[9] Thus the approximation of Ref. 29 even at the high-energy edge may not be much better than the one reported here and contains an unspecified cut-off parameter. In either calculation the shape of the high-energy peak has primarily qualitative significance.

In conclusion, we find that many-body processes have a strong effect on the absolute intensity of soft x-ray emission and also introduce new structures into the spectrum which cannot be attributed to a one-electron density of states. Careful study of the experimental spectra of light metals can thus provide an important means of gaining information about electron correlations in metals as well as a check on theoretical approximation methods. In particular, it would be interesting to have more information about the following features of the spectrum of sodium.

(i) The shape of the main band. How strong is the peak at the high-energy edge? What is its width? And how does it depend on temperature, electron density, and impurities?

(ii) The strength and extent of the low-energy tail of the main band. Can one separate off the purely experimental background from the tail due to electron-electron interactions?

(iii) The shape of the plasmon satellite band. What is the relative magnitude and position of the satellite band as compared to the main band? Does the satellite band show the characteristic $(E_0 - E)^{3/2}$ behavior close to its high-energy edge? Is there any structure due to the plasmaron? Where is it located and how strong? How do these features depend on electron density and temperature?

ACKNOWLEDGMENT

We would like to thank Dr. Pierre Longe for many helpful discussions during the course of this work.

APPENDIX

In this Appendix we calculate the self-energy of the renormalized bound-state propagator.

As seen in Sec. II, there are three distinct processes, shown in Fig. 3(b), which contribute to the self-energy. The first two are electron-electron self-energy and the third is a radiative self-energy. The contribution of the first process can be written as

$$\Sigma_{B1}(\omega) = \frac{1}{2\pi\Omega} \sum_{\vec{k}_a} \sum_{\vec{k}_v} \int d\omega_v \, V(k_v, \omega_v) \times S_F(k_a, \omega - \omega_v) \sum_{i=1}^{3} |f_i(\vec{k}_a + \vec{k}_v)|^2 .$$

We can carry out the ω_v integral very simply and obtain

$$\Sigma_{B1}(\omega) = \frac{1}{\Omega} \sum_{\vec{k}_a} \sum_{\vec{k}_v} [\eta_{\vec{k}_{a>}} V_+(\vec{k}_v, \omega - E_a) - \eta_{\vec{k}_{a<}} V_-(\vec{k}_v, \omega - E_a)] \sum_{i=1}^{3} |f_i(\vec{k}_a + \vec{k}_v)|^2 , \tag{A1}$$

where V_+ and V_- are those parts of the dynamic Coulomb interaction $V(\vec{k}, \omega)$, which are analytic in the upper and lower half of the complex frequency plane, respectively.

Similarly we get for the second process given by Fig. 3(b),

$$\Sigma_{B2}(\omega) = \frac{1}{\Omega} \sum_{\vec{k}_v} V_-(\vec{k}_v, \omega - E_B) \sum_{i,e=1}^{3} |g_{ie}(\vec{k}_v)|^2 , \tag{A2}$$

and the third process gives

$$\Sigma_{B3}(\omega) = \frac{e^2 h^3 \Omega}{12\pi^4 m^2 c} \int d\vec{k}_a \int k_e \, dk_e \times \left(\frac{\eta_{\vec{k}_a >}}{ck_e - \hbar\omega + E_a + i\lambda} + \frac{\eta_{\vec{k}_a <}}{ck_e + \hbar\omega - E_a - i\lambda} \right) \times \sum_{i=1}^{3} |h_{\vec{n},i}(\vec{k}_a)|^2 . \tag{A3}$$

The vertex functions $f_i(\vec{k})$, $h_{\vec{n},i}(\vec{k})$, and $g_{ie}(\vec{k})$ appearing in these equations were defined in I.

First we consider the electron-electron self-energy. As noted in Sec. III, for the purpose of our calculation of the emission intensity the only significant contribution to the imaginary part of the self-energy $\Gamma_B(\omega)$ comes from the second term of Eq. (A1), thus we write

$$\Gamma_B(\omega) = -\frac{1}{(2\pi)^3} \int d\vec{k}_a \int d\vec{k}_v \, \eta_{\vec{k}_a <} \operatorname{Im} V_-(\vec{k}_v, \omega - E_a) \times \sum_{i=1}^{3} |f_i(\vec{k}_a + \vec{k}_v)|^2 . \tag{A4}$$

TABLE III. Frequency dependence of the imaginary part of the bound-state self-energy.

$\frac{\omega}{4E_F}$	$\Gamma_B(\omega)/4E_F$
−2.17	2.157×10^{-4}
−0.40	6.154×10^{-4}
−0.25	4.430×10^{-4}
−0.15	3.354×10^{-4}
−0.10	2.806×10^{-4}
−0.05	2.249×10^{-4}
0.	1.685×10^{-4}
0.05	1.441×10^{-4}
0.10	1.555×10^{-4}
0.15	0.819×10^{-4}
0.20	0.434×10^{-4}
0.25	0.

TABLE IV. Frequency dependence of the real part of the bound-state self-energy.

$\omega/4E_F$	$\Sigma_B(\omega)/4E_F$	$\omega/4E_F$	$\Sigma_B(\omega)/4E_F$
−2.1707	−0.736 395	−1.90	−0.898 042
−2.15	−0.761 307	−1.85	−0.914 012
−2.125	−0.780 218	−1.80	−0.928 094
−2.10	−0.802 178	−1.75	−0.940 626
−2.075	−0.818 532	−1.65	−0.962 004
−2.05	−0.833 145	−1.60	−0.971 208
−2.025	−0.846 363	−1.55	−0.979 604
−2.00	−0.858 423	−1.50	−0.987 290
−1.975	−0.869 500	−1.45	−0.994 375
−1.95	−0.879 727	−1.40	−1.000 912
−1.925	−0.889 213	−1.35	−1.006 988

As in I we can carry out the angular integrations and get

$$\Gamma_B(\omega) = -\frac{1}{\pi} \int_0^\infty z^2 \, dz \int_0^{1/2} da \operatorname{Im} V_- \left(z, \frac{w^2 - a^2}{z} \right) \times M_{B1}(a, z) . \tag{A5}$$

M_{B1} is given by

$$M_{B1}(a, z) = F^2 a^2 [(a^2 + z^2) J_0 + 2J_1] ,$$

where

$$J_0 = \frac{2}{5} \frac{5(a^2 + z^2 + \beta^2)^4 + 10(a^2 + z^2 + \beta^2)^2 (2az)^2 + (2az)^4}{[(a^2 + z^2 + \beta^2)^2 - (2az)^2]^5}$$

and

$$J_1 = -\frac{2}{5} \frac{(a^2 + z^2 + \beta^2)(2az)^2 [5(a^2 + z^2 + \beta^2)^2 + 3(2az)^2]}{[(a^2 + z^2 + \beta^2)^2 - (2az)^2]^5} .$$

$\operatorname{Re}\Sigma_B(\omega)$ can be obtained from the real parts of Eqs. (A1) and (A2). However, it was shown in I that contributions from diagrams of type (A1), containing vertices where a core-hole line, a conduction-band hole line and an interaction line appear, are negligibly small compared to contributions from diagrams of type (A2) containing vertices where two hole lines meet an interaction line. This is physically reasonable because the very large energy involved in the transition of a core hole to a conduction-band hole or vice versa, can hardly be taken into account by the effective Coulomb interaction. Thus $\operatorname{Re}\Sigma_{B2}(\omega)$ takes the form

$$\mathrm{Re}\Sigma_B(\omega)=\frac{G^2}{2\pi^2}\int_0^\infty z^2\,dz\left(\frac{36z^4}{(z^2+4\beta^2)^8}+\frac{1}{(z^2+4\beta^2)^6}-\frac{12z^2}{(z^2+4\beta^2)^7}\right)\frac{6\pi^2c^2}{mz^2}\left(\tfrac{1}{2}-\frac{P}{\pi}\int_{-\infty}^{0}\frac{du}{u-u_s}\,\mathrm{Im}V_-(z,u)\right), \tag{A6}$$

where $u_s=m(\omega-E_B')/k_vk_F$.

The final two-dimensional integrals over a and z in (A5) and the one-dimensional integral over z in (A6) are carried out numerically for different values of the frequency. The results are shown in Tables III and IV. Table III shows that the imaginary part of the bound-state self-energy goes through a broad peak as a function of frequency and vanishes at the Fermi energy. The real part of $\Sigma_B(\omega)$ is negative in the frequency range of our interest. Also observe that both the real and imaginary parts of $\Sigma_B(\omega)$ are very slowly varying functions of ω.

Finally we consider the radiative self-energy given by Eq. (A3). For our purposes it suffices to calculate the width $\Gamma_{B_3}(\omega)=\mathrm{Im}\Sigma_{B_3}(\omega)$ on the energy shell $\hbar\omega=E_B$. Using $h^{\mp}_{\vec{n},t}(\vec{k})$ as given in I and the parameters appropriate to sodium (Appendix A of I) one finds

$$\Gamma_{B\,\mathrm{radiative}}\simeq 0.6\times10^{-6}\ \mathrm{eV}.$$

As seen above the analogous calculation for the Auger width gave

$$\Gamma_{B\,\mathrm{Auger}}\simeq 2.4\times10^{-3}\ \mathrm{eV}\simeq 4000\,\Gamma_{B\,\mathrm{rad}}.$$

Thus we can neglect the radiative width in comparison with the Auger width as stated above in the text.

*Supported in part by the National Science Foundation under Grant No. GP-23571 and in part by the U. S. Air Force Office of Scientific Research under Grant Nos. AF-AFOSR-735-65 and AFOSR 68-1459, to the University of Maryland. The computer time used was supported in part by the National Aeronautics and Space Administration under Grant No. NsG398 to the Computer Science Center of the University of Maryland.

†Based in part on a thesis submitted by S. M. Bose in partial fulfillment of the requirements for the degree of Doctor of Philosophy at the University of Maryland, August, 1967. Preliminary results were first reported at the Conference on Soft X-Ray Spectrometry and the Band Structure of Metals and Alloys, University of Strathclyde, Glasgow, Scotland, 1967 (see Ref. 25).

‡Present address.

[1]P. Longe and A. J. Glick, Phys. Rev. 177, 526 (1969), referred to in the text as I.

[2]G. A. Rooke, Phys. Lett. 3, 234 (1963).

[3]L. Hedin, Solid State Commun. 5, 451 (1967); see also *Soft X-Ray Band Spectra*, edited by D. J. Fabian (Academic, New York, 1968), p. 337.

[4]L. Hedin, B. I. Lundqvist, and S. Lundqvist, Solid State Commun. 5, 237 (1967).

[5]See e.g., R. S. Crisp and S. E. Williams, Philos. Mag. 5, 1205 (1960) and Philos. Mag. 6, 365 (1961).

[6]G. D. Mahan, Phys. Rev. 163, 612 (1967).

[7]B. Roulet, J. Gavoret, and P. Nozieres, Phys. Rev. 178, 1072 (1969).

[8]P. Nozières and C. T. de Dominicis, Phys. Rev. 178, 1097 (1969).

[9]G. A. Ausman, Jr. and A. J. Glick, Phys. Rev. 183, 687 (1969).

[10]The effect of the lifetime of the initial state has been considered by T. McMullen and B. Bergerson, Can. J. Phys. 50, 1002 (1972). They find that the core width causes a smearing of the spectrum, but, since Γ_B is sufficiently small in our case, it will not cause much change in the present results.

[11]B. Bergersen, F. Brouers, and P. Longe, Phys. Rev. B 5, 2385 (1972); J. Phys. F 1, 945 (1971).

[12]K. S. Liu and A. J. Glick, Bull. Am. Phys. Soc. 19, 463 (1974).

[13]K. S. Liu and A. J. Glick (to be published).

[14]G. Baym and L. Kadanoff, Phys. Rev. 124, 287 (1962).

[15]R. G. Rystephanick and J. P. Carbotte, Phys. Rev. 166, 607 (1968).

[16]P. Nozieres, J. Gavoret, and B. Roulet, Phys. Rev. 178, 1084 (1969).

[17]S. M. Bose, A. Bardasis, A. J. Glick, D. Hone, and P. Longe, Phys. Rev. 155, 379 (1967).

[18]B. I. Lundqvist, Phys. Kondens. Mater. 6, 193 (1967); 6, 206 (1967); 7, 117 (1968).

[19]H. W. B. Skinner, Philos. Trans. R. Soc. Lond. A 239, 95 (1940).

[20]P. W. Anderson, Phys. Rev. Lett. 18, 1049 (1967).

[21]W. M. Cady and D. H. Tomboulian, Phys. Rev. 59, 381 (1941).

[22]R. A. Ferrell, Phys. Rev. 186, 128 (1969).

[23]See e.g., J. P. Carbotte, and S. Kahana, Phys. Rev. 139, A213 (1965).

[24]R. A. Ferrell, Technical Report No. 485, University of Maryland, 1965 (unpublished).

[25]The $(E_0-E)^{3/2}$ behavior for the first-order theory was observed in this way by G. A. Ausman, Jr. (private communication).

[26]Note that this peak occurs at an energy different from the one obtained by Hedin. This is because in the calculation of the plasmon satellite band, we approximated $\Sigma_1(\vec{k},\omega)$ by the one obtained by using Eq. (12) where $\Sigma_2(\vec{k},\omega)$ was replaced by Σ_2 plasmon $(\vec{k},\omega)$ (see Ref. 13). A more careful evaluation of $\Sigma_1(\vec{k},\omega)$ would bring these peaks closer.

[27]J. R. Cuthill, R. C. Dobbyn, A. J. McAlister, and M. L. Williams, Phys. Rev. 174, 515 (1968).

[28]A. J. Glick, P. Longe, and S. M. Bose, *Soft X-Ray Band Spectra*, edited by D. J. Fabian (Academic, 1968), pp. 319–328 (conference proceedings).

[29]A. Morita and M. Watabe, J. Phys. Soc. Jap. 25, 1060 (1968).

[30]P. T. Landsberg, Proc. Phys. Soc. Lond. A 62, 806 (1949); also see Ref. 1 above.